Dalton Transactions

ROYAL SOCIETY OF CHEMISTRY

COMMUNICATION

View Article Online
View Journal | View Issue

Cite this: *Dalton Trans.*, 2021, **50**, 3459

Received 11th January 2021,
Accepted 15th February 2021

DOI: 10.1039/d1dt00091h

rsc.li/dalton

Formation of a tris(catecholato) iron(III) complex with a nature-inspired cyclic peptoid ligand†

Jinyoung Oh,‡[a] Dahyun Kang,‡[a] Sugyeong Hong,[b] Sun H. Kim,[b] Jun-Ho Choi[a] and Jiwon Seo *[a]

Siderophore-mimicking macrocyclic peptoids were synthesized. Peptoid 3 with intramolecular hydrogen bonds showed an optimally arranged primary coordination sphere leading to a stable catecholate-iron complex. The tris(catecholato) structure of 3-Fe(III) was determined with UV-vis, fluorescence, and EPR spectroscopies and DFT calculations. The iron binding affinity was comparable to that of deferoxamine, with enhanced stability upon air exposure.

Iron is an essential element in living organisms and plays vital roles in redox processes such as N_2 fixation,[1] oxygenation,[2] respiration[3] and photosynthesis.[4] Nonetheless, free iron is very toxic under aerobic conditions and produces reactive oxygen species through various processes, such as the Fenton reaction.[5] Ferrous and ferric ions are poorly soluble in aqueous media since they easily form hydroxide complexes.[6] To circumvent these problems, nature utilizes various iron-binding systems, such as transferrin, ferritin, and siderophores.

Microorganisms utilize siderophores as a crucial iron-transporting system. Siderophores have a high iron binding affinity to facilitate intracellular iron uptake from an iron-poor environment (aqueous solution) and have a low molecular weight to make the process efficient and economic. In particular, siderophores with tris(catecholato) iron complexes exhibit remarkable stability constants compared with other siderophores based on hydroxamates or carboxylates.[7,8] For example, the stability constant of enterobactin is the highest among those of all existing iron-binding ligands known to date (Fig. 1). This finely optimized iron-transport system has been applied in, for example, iron chelation therapy[9] and sideromycin.[10]

For bacteria, backbone lability through enzymatic hydrolysis is a required aspect for intracellular release of iron; however, this lability often undermines the stability of these iron complexes.[11,12] To overcome this problem, synthetic iron chelators have been developed using iron-chelating moieties displayed on abiotic macrocyclic backbones[13,14] or without a backbone.[15,16] Among the unnatural scaffolds actively investigated for metal chelation are peptoids.[17,18] Peptoids have a *N*-substituted glycine backbone, a structure isomeric to that of natural peptides, and are resistant to degradation by hydrolytic enzymes. The chemical diversity of peptoids is large because of the readily available primary amine submonomers,[19] allow-

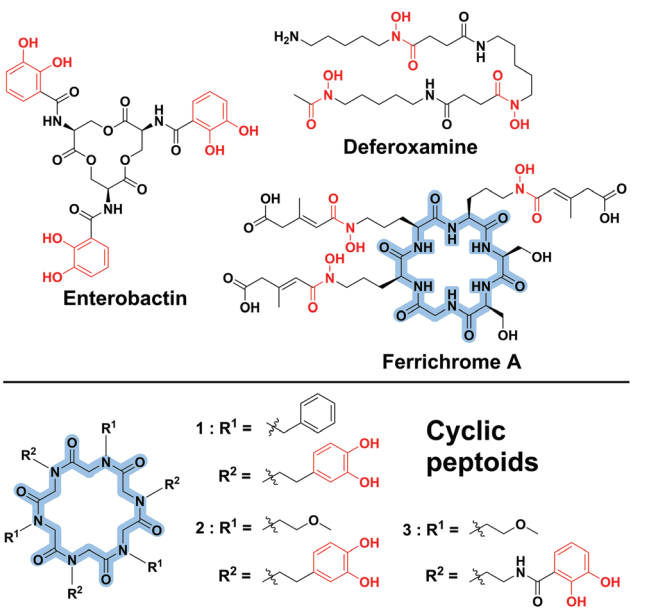

Fig. 1 Natural siderophores and catechol-containing cyclic peptoids **1–3**. Iron-chelating motifs are colored red and hexameric skeletons are colored blue.

[a]*Department of Chemistry, School of Physics and Chemistry, Gwangju Institute of Science and Technology, 123 Cheomdangwagi-ro, Buk-gu, Gwangju, 61005, Republic of Korea. E-mail: jseo@gist.ac.kr*
[b]*Western Seoul Center, Korea Basic Science Institute, University-Industry Cooperation Building, 150 Bukahyun-ro, Seodaemun-gu, Seoul, 120-140, Republic of Korea*

†Electronic supplementary information (ESI) available. See DOI: 10.1039/d1dt00091h

‡These authors contributed equally to this work.

ing peptoids to serve as highly modular scaffolds for chemical diversification.

In this work, we employed a cyclic hexapeptoid scaffold to display an iron-binding catechol moiety. A tris(catecholato) system attached to the macrocyclic peptoid demonstrated the importance of the orientation of the two hydroxyl groups in the catechol moiety and the neighboring hydrogen bond to stabilize the iron complex, reminiscent of the structural characteristics of enterobactin. Our synthetic siderophore-iron complex exhibited an optimally arranged primary coordination sphere, leading to a stable iron complex.

Three macrocyclic peptoids that mimic natural siderophores were synthesized (Fig. 1). The design of the cyclic skeleton (*i.e.*, ring size) and the chelating arms (*i.e.*, catecholate) was based on ferrichrome and enterobactin, respectively. Compounds **1** and **2**, both of which have dopamine moieties as catecholate ligands, were prepared and exhibited different hydrophilicities as a result of their extra ligands: benzyl and methoxyethyl groups. The amide group was incorporated into the chelating arms of compound **3** to increase the stability of the metal complex by hydrogen bonding between the amide proton and catecholate, a strategy also utilized by enterobactin.[20–22]

The sequence of the linear peptoid was elongated on a 2-chlorotrityl chloride resin by following the peptoid submonomer synthesis protocol.[19] A catechol-containing submonomer (R'-NH_2) protected by either an acetonide or a benzyl group was used (Schemes S1 and S2†).[23–25] After elongation, a cleavage reaction using a mildly acidic cocktail (TFE/TIS/CH_2Cl_2 = 1 : 1 : 8, v/v/v) yielded a linear peptoid with high purity, which then underwent head-to-tail cyclization using previously optimized conditions, with modification of only the solvent to CH_2Cl_2 for simpler evaporation.[26] Kirshenbaum and coworkers suggested that the macrocyclization reaction was most effective when the linear peptoid was a hexamer, as in our synthesis.[26] The cyclic peptoids were deprotected and purified by preparative HPLC to afford compounds **1–3** (Scheme 1). All reactions in Scheme 1 were monitored by analytical HPLC and ESI-MS, and the final cyclic peptoids **1–3** were obtained with purity greater than 98% (Fig. S1†).

The Fe(III) binding mode of the peptoid was verified by UV-vis spectral analysis and fluorescence quenching experiments.

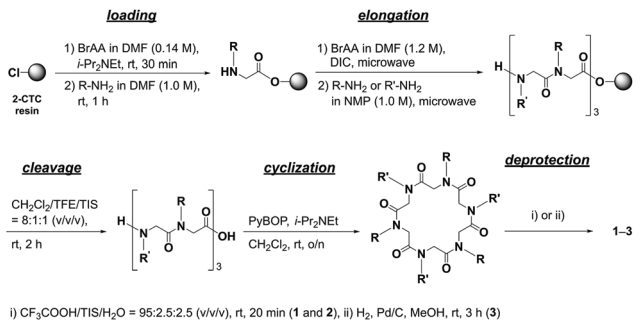

Scheme 1 Synthetic route for cyclic peptoids **1–3**.

Catechol-iron complexes are known to have different binding stoichiometries depending on the concentration of base and Fe(III), as demonstrated by their different UV-vis spectral signatures.[27,28] For catechol-iron complexes, each bis- and tris-complex has absorption maxima at approximately 570 nm and 480 nm respectively.[29] Recently, De Riccardis and coworkers reported an enterobactin/bacillibactin-mimic cyclic tripeptoid and showed the formation of a dinuclear bis(catecholato) iron (III) complex with an absorption maximum at approximately 570 nm.[30] The base titration of our cyclic peptoids was performed for iron binding mode characterization. In methanol and in the absence of base, peptoids **1** and **2** did not show any distinct peak attributed to iron complex formation (Fig. S2,† Fig. 2A). Upon addition of six equivalents of NaOH, which can deprotonate the six acidic protons on the three catechols, peptoids **1** and **2** appeared to form bis-complexes. These complexes showed a gradual transition (bis- to tris-complex) as the number of equivalents of base increased. On the other hand, peptoid **3** formed a bis-complex in the absence of a base and in the presence of up to six equivalents of NaOH, and a bis- to tris-complex transition occurred in methanol as the amount of added base increased (Fig. 2B). Interestingly, in acetonitrile, the absorption maximum of the tris-complex appeared at approximately 480 nm without any base and was saturated by 6 equivalents of Et_3N (Fig. 2C). This finding can be explained by the stability of the tris-complex conferred by the hydrogen bond between the catechol and neighboring amide –NH protons in an aprotic solvent. This structural aspect will be further discussed below. After the formation of a stable tris-complex in acetonitrile was observed, a fluorescence quenching experiment was performed to elucidate the binding stoichiometry of the **3**-Fe(III) complex. Emission of the dihydroxy-

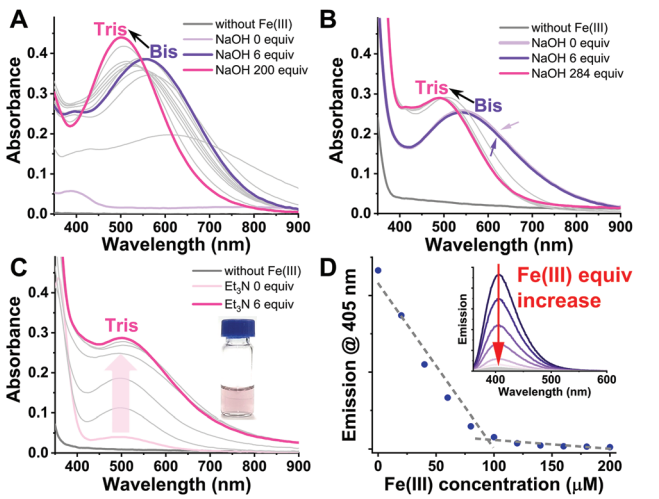

Fig. 2 Spectral characterization of Fe(III)-binding cyclic peptoids. UV-vis spectra of $Fe(NO_3)_3{\cdot}9H_2O$ (100 μM) and solutions of (A) **2** (100 μM) and (B) **3** (100 μM) in methanol titrated with NaOH(aq). (C) UV-vis spectra of $FeCl_3$ (100 μM) and **3** (100 μM) solutions in acetonitrile titrated with Et_3N. (D) Plot of the fluorescence titration result for **3** (100 μM) with $Fe(acac)_3$ in acetonitrile (λ_{ex} = 350 nm/λ_{em} = 405 nm).

benzene chromophore at approximately 400 nm was observed upon excitation at 350 nm,[31] and evidence of iron complex formation was previously provided by quantitative fluorescence quenching.[32] At a fixed concentration of **3**, the fluorescence of the catechol chromophore was linearly quenched as the concentration of Fe(III) increased (Fig. 2D, inset), and the quenching effect by the addition of Fe(III) was completed at a ratio of 1 : 1 (Fig. 2D). It should be noted that the counterion of Fe(III) affected the titration results, as was previously observed.[33,34] The experiment with $FeCl_3$ resulted in a nonlinear quenching tendency (Fig. S3†), whereas the Fe(III) complex with acetylacetonate (acac) showed linear quenching, providing a clear binding ratio.

The natural siderophore-Fe(III) complex has unique EPR absorption (g_{eff} = 4.3), which is used as a signature to identify nonheme high-spin iron(III).[35–37] The presence of multiple unpaired electrons, such as in a high-spin d^5 system, leads to splitting of the electronic state in the absence of a magnetic field, called zero-field splitting (ZFS). As the electronic state splits, the states become highly mixed, and intra-Kramers transitions become allowed. The result of an intra-Kramers transition from the $|\pm 3/2>$ Kramers doublet appeared as a strong absorption at 1550 G, with a g_{eff} value of 4.3 (Fig. 3A). This iron in the complex is also called rhombic iron, which possesses rhombic (distorted octahedral) symmetry. Further insight was subsequently obtained through EPR spectrum simulation with EasySpin toolbox 5.2.27,[38] which provided the ZFS tensor value as a rhombicity (E/D) of 0.31 (E/D_{axial} = 0 and $E/D_{rhombic}$ = 1/3). This decisive information clarified that iron exists as a high-spin ion in the hexadentate nonheme environment with rhombic symmetry, similar to that in the natural enterobactin-iron(III) complex.

Based on the EPR analysis, DFT calculations were performed to visualize the structure of the **3**-Fe(III) complex with high-spin ($^6S_{5/2}$; sextet) iron and a net charge of −3 (Fig. 3B). The iron atom was treated by the effective core potential basis set LANL2DZ to reduce computational effort. The geometry of the **3**-Fe(III) complex was optimized in the condensed phase using a self-consistent reaction field. The primary coordination sphere of the complex was optimized with a rhombic geometry. The distance between the oxygen atom of the catecholate and the Fe(III) ion was in the range of 2.02–2.11 Å. In accordance with a previous study on ferric enterobactin, the length of the Fe–O_{ortho} bonds was slightly longer (2.09–2.11 Å) than that of the Fe–O_{meta} bonds (2.02–2.03 Å) (Ent-Fe(III): Fe–O_{ortho} 2.03–2.04 Å; Fe–O_{meta} 1.97–2.02 Å) due to hydrogen bonding.[22] In the secondary coordination sphere, intramolecular hydrogen bonding was confirmed by the H···O distance of 1.80 Å (Ent-Fe(III): 1.73 Å).[22] The resulting parameters revealed that the **3**-Fe(III) complex has a distorted octahedral primary sphere with intramolecular hydrogen bonding between the amide proton and catecholate oxygen in the secondary coordination sphere.

The iron binding affinity of **3** was estimated through a competitive Fe(III) binding assay with ethylenediamine-tetraacetic acid (EDTA) (Fig. 4). Known iron-binding ligands, including deferiprone (DFP), 3,4-dihydroxybenzoic acid (3,4-DHBA), deferoxamine (DFO), and enterobactin (Ent), were used to compare the binding affinity. The iron complex formation constants in aqueous buffer were as follows: EDTA ($\beta = 10^{25}$),[39] DFP ($\beta = 10^{15}$),[40,41] 3,4-DHBA ($\beta = 10^{5}$),[42] DFO ($\beta = 10^{31}$),[43] and Ent ($\beta = 10^{49}$).[7] Although the **3**-Fe(III) complex was soluble in water, the peptoid ligand itself was not soluble in aqueous media. Thus, the formation constant of peptoid **3** could not be directly measured, and the competition assay was performed in an acetonitrile/water = 9 : 1 (v/v) mixture instead. As shown in Fig. 4, the natural siderophore Ent showed remarkable stability of the iron complex. In contrast, a dramatic loss of Fe(III) complexed with DFP and 3,4-DHBA was observed after the addition of 1.5 equivalents (150 μM) of EDTA. Competitive iron binding affinity was observed for another natural siderophore, DFO, and peptoid **3**, which showed iron binding affinity comparable to that of DFO. Regarding long-term stability, the **3**-Fe(III) complex appeared to be more stable than the DFO-Fe(III) complex (Fig. S4†). Cyclic voltammetry measurements suggested the stability of the **3**-Fe(III) complex with a defined structure under basic conditions over −1.5–1.5 V *vs.* Ag/Ag^+ (Fig. S5†). Without the addition of a base, the **3**-Fe(III) complex

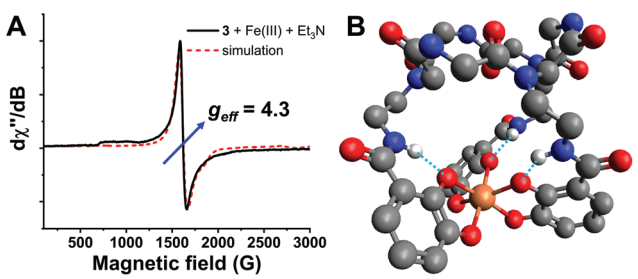

Fig. 3 (A) EPR spectrum experimentally measured for the **3**-Fe(III) complex in acetonitrile at 5 K (solid black line) and obtained by simulation (dashed red line). (B) DFT-calculated structure of the **3**-Fe(III) complex (B3LYP/6-31g+(d,p); LANL2DZ for Fe) under acetonitrile solvation conditions. Hydrogen atoms except for the amide protons and methoxyethyl side chains are omitted for clarity.

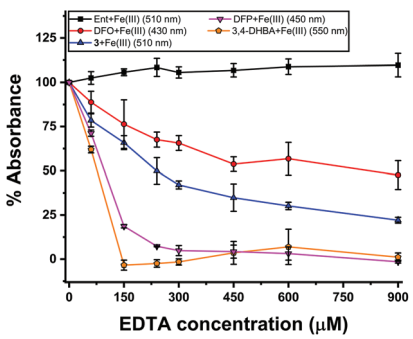

Fig. 4 Competitive Fe(III) binding assay with EDTA for the evaluation of the iron binding affinity. The absorbance of the compounds without EDTA was set as 100%, and all samples were prepared at a concentration of 100 μM in an acetonitrile/water = 9 : 1 (v/v) solution.

became unstable in the redox environment, likely due to the occurrence of a cross-linking reaction[44] upon application of the reductive potential (Fig. S6†).

In summary, we report the synthesis of cyclic peptoid-Fe(III) complexes and their characterization by UV-vis spectroscopy, fluorescence spectroscopy, EPR spectroscopy, and DFT calculations. Simple display of three catechols on cyclic peptoids (**1** and **2**) did not lead to the formation of a stable tris(catecholato) iron(III) complex. Mimicking the natural siderophore enterobactin, incorporation of amide next to the catechol and orienting two hydroxyls toward the center of the macrocycle led to successful formation of the tris(catecholato) iron(III) complex. The **3**-Fe(III) complex demonstrated the importance of intramolecular hydrogen bonds between amide protons and catechol oxygen atoms to stabilize the tris-complex with a 1 : 1 stoichiometry. An increased ring size compared to that of enterobactin led to decreased iron affinity; however, the three extra residues left room for further chemical diversification or conjugation with other bioactive molecules. Our peptoid-Fe(III) complex may expand the field of siderophore mimicry toward novel sideromycin design or antibiotic strategies by nutritional immunity.[45]

Conflicts of interest

There are no conflicts of interest to declare.

Acknowledgements

This work was financially supported by the National Research Foundation of Korea (NRF-2018R1A2B6007535) and by the Creative Materials Discovery Program (NRF-2018M3D1A1052659), which is funded by the National Research Foundation (NRF) under the Ministry of Science and ICT. The authors are also grateful to the Korean Basic Science Institute (KBSI) in Gwangju for instrumentation support (^{1}H and ^{13}C NMR measurements).

Notes and references

1 M. Georgiadis, H. Komiya, P. Chakrabarti, D. Woo, J. Kornuc and D. Rees, *Science*, 1992, **257**, 1653–1659.
2 D. H. Ohlendorf, J. D. Lipscomb and P. C. Weber, *Nature*, 1988, **336**, 403–405.
3 T. Tsukihara, H. Aoyama, E. Yamashita, T. Tomizaki, H. Yamaguchi, K. Shinzawa-Itoh, R. Nakashima, R. Yaono and S. Yoshikawa, *Science*, 1995, **269**, 1069–1074.
4 J. Deisenhofer, O. Epp, K. Miki, R. Huber and H. Michel, *J. Mol. Biol.*, 1984, **180**, 385–398.
5 B. Halliwell and J. M. C. Gutteridge, *Biochem. J.*, 1984, **219**, 1–14.
6 R. M. Smith and A. E. Martell, *Sci. Total Environ.*, 1987, **64**, 125–147.
7 L. D. Loomis and K. N. Raymond, *Inorg. Chem.*, 1991, **30**, 906–911.
8 E. A. Dertz, J. D. Xu, A. Stintzi and K. N. Raymond, *J. Am. Chem. Soc.*, 2006, **128**, 22–23.
9 C. B. Modell and J. Beck, *Ann. N. Y. Acad. Sci.*, 1974, **232**, 201–210.
10 M. Ghosh, P. A. Miller, U. Möllman, W. D. Claypool, V. A. Schroeder, W. R. Wolter, M. Suckow, H. Yu, S. Li, W. Huang, J. Zajicek and M. J. Miller, *J. Med. Chem.*, 2017, **60**, 4577–4583.
11 R. J. Abergel, A. M. Zawadzka, T. M. Hoette and K. N. Raymond, *J. Am. Chem. Soc.*, 2009, **131**, 12682–12692.
12 F. Ecker, H. Haas, M. Groll and E. M. Huber, *Angew. Chem., Int. Ed.*, 2018, **57**, 14624–14629.
13 E. J. Corey and S. D. Hurt, *Tetrahedron Lett.*, 1977, **18**, 3923–3924.
14 Q. Zhang, B. Jin, Z. Shi, X. Wang, Q. Liu, S. Lei and R. Peng, *Sci. Rep.*, 2016, **6**, 34024.
15 F. L. Weitl and K. N. Raymond, *J. Am. Chem. Soc.*, 1979, **101**, 2728–2731.
16 U. Möllmann, A. Ghosh, E. K. Dolence, J. A. Dolence, M. Ghosh, M. J. Miller and R. Reissbrodt, *BioMetals*, 1998, **11**, 1–12.
17 M. Baskin and G. Maayan, *Biopolymers*, 2015, **104**, 577–584.
18 K. J. Prathap and G. Maayan, *Chem. Commun.*, 2015, **51**, 11096–11099.
19 R. N. Zuckermann, J. M. Kerr, S. B. H. Kent and W. H. Moos, *J. Am. Chem. Soc.*, 1992, **114**, 10646–10647.
20 T. B. Karpishin and K. N. Raymond, *Angew. Chem., Int. Ed.*, 1992, **31**, 466–468.
21 K. N. Raymond, E. A. Dertz and S. S. Kim, *Proc. Natl. Acad. Sci. U. S. A.*, 2003, **100**, 3584–3588.
22 T. C. Johnstone and E. M. Nolan, *J. Am. Chem. Soc.*, 2017, **139**, 15245–15250.
23 Z. Liu, B.-H. Hu and P. B. Messersmith, *Tetrahedron Lett.*, 2010, **51**, 2403–2405.
24 R. A. Gardner, R. Kinkade, C. Wang and O. Phanstiel IV, *J. Org. Chem.*, 2004, **69**, 3530–3537.
25 S. Lei, B. Jin, Q. Zhang, Z. Zhang, X. Wang, R. Peng and S. Chu, *Polyhedron*, 2016, **119**, 387–395.
26 S. B. Y. Shin, B. Yoo, L. J. Todaro and K. Kirshenbaum, *J. Am. Chem. Soc.*, 2007, **129**, 3218–3225.
27 N. Holten-Andersen, M. J. Harrington, H. Birkedal, B. P. Lee, P. B. Messersmith, K. Y. C. Lee and J. H. Waite, *Proc. Natl. Acad. Sci. U. S. A.*, 2011, **108**, 2651–2655.
28 H. Zeng, D. S. Hwang, J. N. Israelachvili and J. H. Waite, *Proc. Natl. Acad. Sci. U. S. A.*, 2010, **107**, 12850–12853.
29 M. J. Sever and J. J. Wilker, *Dalton Trans.*, 2004, **7**, 1061–1072.
30 A. D'Amato, P. Ghosh, C. Costabile, G. Della Sala, I. Izzo, G. Maayan and F. De Riccardis, *Dalton Trans.*, 2020, **49**, 6020–6029.
31 Rahmi and H. Itagaki, *J. Photopolym. Sci. Technol.*, 2011, **24**, 517–521.
32 N. Guo, X. You, Y. Wu, D. Du, L. Zhang, Q. Shang and W. Liu, *Anal. Chem.*, 2020, **92**, 5780–5786.

33 L. A. Actis, W. Fish, J. H. Crosa, K. Kellerman, S. R. Ellenberger, F. M. Hauser and J. Sanders-Loehr, *J. Bacteriol.*, 1986, **167**, 57–65.
34 H. Lee, W. Y. Song, M. Kim, M. W. Lee, S. Kim, Y. S. Park, K. Kwak, M. H. Oh and H. J. Kim, *Org. Lett.*, 2018, **20**, 6476–6479.
35 H. H. Wickman, M. P. Klein and D. A. Shirley, *J. Chem. Phys.*, 1965, **42**, 2113–2117.
36 K. Spartalian, W. Oosterhuis and J. Neilands, *J. Chem. Phys.*, 1975, **62**, 3538–3543.
37 F. Bou-Abdallah and N. D. Chasteen, *JBIC, J. Biol. Inorg. Chem.*, 2008, **13**, 15–24.
38 S. Stoll and A. Schweiger, *J. Magn. Reson.*, 2006, **178**, 42–55.
39 R. M. Smith and A. E. Martell, *Sci. Total Environ.*, 1987, **64**, 125–147.
40 R. J. Motekaitis and A. E. Martell, *Inorg. Chim. Acta*, 1991, **183**, 71–80.
41 E. T. Clarke and A. E. Martell, *Inorg. Chim. Acta*, 1992, **191**, 57–63.
42 J. Kennedy and H. Powell, *Aust. J. Chem.*, 1985, **38**, 659–667.
43 G. Schwarzenbach and K. Schwarzenbach, *Helv. Chim. Acta*, 1963, **46**, 1390–1400.
44 M. Yu, J. Hwang and T. Deming, *J. Am. Chem. Soc.*, 1999, **121**, 5825–5826.
45 P. Thulasiraman, S. M. C. Newton, J. Xu, K. N. Raymond, C. Mai, A. Hall, M. A. Montague and P. E. Klebba, *J. Bacteriol.*, 1998, **180**, 6689–6696.